Abstract

Measurement of total hadronic differential cross sections in the LArIAT experiment

Elena Gramellini

2018

Abstract goes here. Limit 750 words.

Measurement of total hadronic differential cross sections in the LArIAT experiment

A Dissertation
Presented to the Faculty of the Graduate School
of
Yale University
in Candidacy for the Degree of
Doctor of Philosophy

by
Elena Gramellini

Dissertation Director: Bonnie T. Fleming

Date you'll receive your degree

Contents

Acknowledgements

A lot of people are awesome, especially you, since you probably agreed to read this when it was a draft.

Chapter 0

Liquid Argon Detectors at the Intensity Frontier

In the next few years, LArTPCs will be the tools to answer some of the burning questions in neutrino physics today. This section illustrates the operational principles of this detector technology, as well as the scope of the key detectors in the US liquid argon program – SBN, DUNE and LArIAT.

0.1 The Liquid Argon Time Projection Chamber Technology

0.1.1 TPCs, Neutrinos & Argon

David Nygren designed the first Time Projection Chamber (TPC) in the late 1970s [15] for the PEP-4 experiment, a detector apt to study electron-positron collisions at the PEP storage ring at the SLAC National Accelerator Laboratory. From the original design in the seventies – a cylindrical chamber filled with methane gas – the TPC detector concept has seen many incarnations, the employment of several different active media and a variety of different particle physics applications, including, but

not limited to the study of electron/positron storage rings (e.g. PEP4, TOPAZ, ALEPH and DELPHI), heavy ions collisions in fixed target and collider experiments (e.g. EOS/HISS and ALICE), dark matter (ArDM), rare decays and capture (e.g. TRIUMP, MuCap), neutrino detectors and nucleon decay (ICARUS, SBN, DUNE), and neutrino less double beta decay (Next). A nice review of the history of TPCs and working principles is provided in [44].

Several features of the TPC technology make these detectors a more versatile tool compared to other ionization detectors and explain such a wide popularity. TPCs are the only electronically read detector which deliver simultaneous three-dimensional track information and a measurement of the particle energy loss. Leveraging on both tracking and calorimetry, particle identification (PID) capabilities are enhanced over a wide momentum range.

Carlo Rubbia first proposed the use of a Liquid Argon TPC for a neutrino experiment, ICARUS [14], in 1977. The active medium in ionization detector has historically been in the gaseous form. Nevertheless, using nobles elements in the liquid form for neutrino detectors is advantageous for several reasons. The density of liquids is ∼1000 times greater than gases, increasing the number of target centers for neutrino's interaction in the same volume. Since the energy loss of charged particle is proportional to the target material density, as shown in the Bethe-Block equation in 1, the increased density reflects into a proportionally higher energy loss, enhancing the calorimetry capability of detectors with a liquid active medium. Additionally, the ionization energy of liquids is smaller than gasses by the order of tens of eV. Thus, at the passage of charged particles, liquid generally produce more ionization electrons than gas for the same deposited energy and force the particles to deposit more energy in a shorter range. The downside of using noble liquid gasses in experiments is that they require a cryogenic system to cool the gas until it transitions to its the liquid form. The properties of liquid argon in comparison liquid xenon – a popular choice for

2

Element	LAr	LXe
Atomic Number	18	54
Atomic weight A	40	131
Boiling Point Tb at 1 atm	87.3 K	165.0 K
Density	1.4 g/cm^3	3.0 g/cm^3
Radiation length	14.0 cm	2.8 cm
Moliere Radius	10.0 cm	5.7 cm
Work function	23.6 eV	15.6 eV
Electron Mobility at $E_{field} = 10^4$ V/m	0.047 m^2/Vs	0.22 m^2/Vs
Average dE/dx MIP	2.1 MeV/cm	3.8 MeV/cm
Average Scintillation Light Yield	40000 γ/MeV	42000 γ/MeV
Scintillation λ	128 nm	175 nm

Table 1: LAr, LXe summary of properties relevant for neutrino detectors.

dark matter and neutrinoless double beta decay detectors – are summarized in table 1. Albeit xenon would be more desirable than argon given some superior properties such as lower ionization energy and higher density and light yield, argon relative abundance abates the cost of argon compared to xenon, making argon a more viable choice for the construction of big neutrino detectors.

LArTPCs are some times referred as to "electronic" bubble-chambers, for the similarity in the tracking and energy resolution which is coupled with an electronic readout of the imaging information in LArTPCs. Compared to these historic detectors however, LArTPC bestow tridimensional tracking and a self triggering mechanism provided by the scintillation light in the noble gas. A comparison between a neutrino interaction in the ArgoNeut LArTPC and in the bubble chamber is shown in picture EVENT DISPLAY.

0.1.2 LArTPC: Principles of Operation

To the bare bones, a LArTPC is a bulk of liquid argon sandwiched in a flat capacitor, equipped with a light collection system. A uniform electric field of the order of 500 V/cm is maintained constant between the faces of the capacitor. The anode is sensitive to ionization charge and it is usually made of two or more planes segmented

into several hundreds parallel sense wires a few millimeters apart; different geometries for the anode segmentation are under study [21].

Argon ionization and scintillation are the processes leveraged to detect particles in the LArTPC active volume. When a ionizing radiation traverses the argon active volume it leaves a trail of ionization electrons along its trajectory and it excites the argon, leading to the production of scintillation light – details on the production and detection of ionization charge and scintillation light are provided in 0.1.4 and 0.1.4 respectively. The optical part of the detector collects the argon scintillation light in matters of nanoseconds. This flash of light determines the start time of an event in the chamber, t_0. The uniform electric field drifts the ionization electrons from the production point towards the anode plane in order of hundreds of microseconds or more depending on the chamber dimensions[1]. The anode sense wires see either an induced current by the drifting charge (on induction planes) or an injection of the ionization charge (collection plane) [94]. An appropriate choice of the voltage bias on each wire plane assures ideal charge transparency, so that all the ionization charge is collected on the collection plane and none on the induction planes [95].

The arrival time of the charge on the anode sense wires is used to measure the position of the original ionizing radiation in the drift direction. In fact, since the constant electric field implies that the drift velocity is also constant in the chamber, the position of the original ionization is simply given by the multiplication of the drift velocity by the drift time, where we define as "drift time" the difference between t_0 and the charge arrival time on the wire planes. The spacial resolution on this dimension is limited by the time resolution of the electronics or by longitudinal diffusion of the electrons. The spatial information on the different wire planes maps a bi-dimensional

---

1. The ionized argon also drifts, but in the opposite directions compared to the electrons. Since the drift time is proportional to the particle mass, the ions drift time is much longer than the electrons'. Ionized argon is collected on the cathode which is not instrumented, so it is not used to infer information about the interactions in the chamber.

projection of the interaction pattern in the plane perpendicular to the drift direction. The spacial resolution on this dimension is limited by the transverse electron diffusion in argon and by the grain of the anode segmentation, i.e. the spacing between the wires in the sense planes [100]. The off-line combination of the 2-D information on the wire planes with the timing information allows for the 3D reconstruction of the event in the chamber.

Since the charge deposited by the ionizing radiation in the chamber is proportional to the deposited energy and the charge collected on the sense plane is a function of the deposited charge, LArTPC allow the measurement of the energy deposit in the active volume. Effects due to the presence of free charge and impurities in the active volume, such as a finite electron lifetime, recombination and space charge, complicate the relationship between deposited and collected charge affecting the measurement of the particle's energy, as described in the next section.

0.1.3   Liquid Argon: Ionization Charge

$$-\frac{dE}{dx} = K z^2 \frac{Z}{A} \varrho \frac{1}{\beta^2} \left[\frac{1}{2} \ln \frac{2 m_e c^2 \beta^2 \gamma^2 T_{max}}{I^2} - \beta^2 - \frac{\delta}{2} \right]$$

Purity & Electron Life Time

The presence of electronegative contaminants in liquid argon, such as oxygen and water, is particularly pernicious, since these molecules quench the charge produced by the ionizing radiation. Thus, amount of charge per unit of length dQ/dx collected on the collection plane depends on the charge's production point in the detector: a ionization produced close to the cathode will see more impurities along its journey to the collection plane than ionization produced close to the anode, resulting in greater attenuation. As a result, the amount of charge collected on the sense wires as a function of the traveled distance follows an exponential decay trend. The traveled

distance is generally measured in terms of drift time and the characteristic time constant of the exponential decay is called electron lifetime τ_e. Figure **??** shows the typical life time for LArIAT data cite technote. LArIAT small drift distance (47 cm) allows for a relatively short electron life time. The life time for bigger detectors such as MicroBooNE, whose drift distance is 2.5 m, needs to be of the order of to allow charge collection usable for physics analyses. Energy reconstruction in LArTPC applies a correction for the finite lifetime to calibrate the detector calorimetric response; details for LArIAT are provided in Section **??**.

LArTPCs use hermetically sealed and leak-checked vessels to abate the leakage and diffusion of contaminants into the system. The liquid argon filling of the volume occurs after the vessel is evacuated or purged with gaseous argon [205] to reduce remaining gases in the volume. Even so, the construction of a pure tank of argon is unviable, as several sources of impurity remain. In particular, impurities can come from the raw argon supply, the argon filtration system and from the outgassing from internal surfaces. Outgassing is a continuous diffusive process producing contaminants, especially water, even after the vessel is sealed, particularly from materials in the ullage region[2]. Since research-grade argon comes from the industrial distillation of air, the impurities with the highest concentration are nitrogen, oxygen and water, generally maintained under the 1 part per million level by the vendor. Even so, a higher level of purity is necessary to achieve a free electron life time usable in meter scale detectors. Thus, argon is constantly filtered in the cryogenic system, which reduce the oxygen and water contamination to less than 100 parts per trillion. The filtration system depends on the size and drift distance of the experiment and, for experiments on several meters scale, it includes an argon recirculation system.

---

2. . While the liquid argon low temperature reduces outgassing in the liquid, this process remains significant for absorptive material (such as plastic) above the surface of the liquid phase

Recombination Effect

After production, ionization electrons thermalize with the surrounding medium and may recombine with nearby ions. Recombination might occur either between the electron and the parent ion through Coulomb attraction (Onsager geminate theory [2]) or thanks to the collective charge density of electrons and ions from multiple ionizations in a cylindrical volume surrounding the particle trajectory (Jaffe[3] columnar model). Consideration on the average electron-ion distance and the average ion-ion distance for argon show that the probability of geminate recombination is low; thus recombination in argon is mainly due to collective effects [?]. Since protons, kaons and stopping particles present a higher ionization compared to MIPs, recombination effects are more prominent when considering the reconstruction of energy deposited by these particles.

Models for a theoretical descriptions of recombination base on are provided in (Birks model [6]) and in (Box model [7]). The Birks model assumes a gaussian spatial distribution around the particle trajectory during the entire recombination phase and identical charge mobility for ions and electrons. The Box model also assumes that electron diffusion and ion mobility are negligible in liquid argon during recombination In these models, the fraction of ionization electrons surviving recombination is a function of the number of ion-electron pairs per unit length, the electric field, the average ion-electron separation distance after thermalization and the angle of the particle with respect to the direction of the electric field – plus the diffusion coefficient in the Birks model. Given the stringent assumptions, it is perhaps not surprising that these models are in accordance to data only in specific regimes: the Birks model is generally used to describe recombination for low dE/dx, the Box model for high dEdX. In LArTPC, the ICARUS and ArgoNeut have measured recombination in [8] and [?] respetively. Since LArIAT uses the refurbished ArgoNeut TPC and cryostat, LArIAT currently corrects for recombination using the ArgoNeut measurement,

shown in figure find figure.

Space Charge Effect

Slow-moving positive argon ions created during ionization can build-up in LArTPC, causing the distortion of the electric field within the detector. This effect, called "space charge effect" leads to a displacement in the reconstructed position of the signal ionization electrons. In surface LArTPCs the space charge effect is primarily due to the rate of ionization produced by cosmic rays which is slowly drifting in the chamber at all times. Surface LArTPC of the size of several meters are expected to be modestly impacted from the space charge effect, where charge build-up create anisotropy of the electric field magnitude of the order of 5% at a drift field of 500 V/cm. The smallness of the LArIAT drift volume is such that effect of space charge on the electric field is expected to b even smaller. CHIEDI A FLAVIO

0.1.4 Liquid Argon: Scintillation Light

Liquid argon emits scintillation light at the passage of charged particles. LArTPCs leverage this property to determine when the ionization charge begins to drift towards the anode plane.

Scintillation Process

Scintillation light in argon peaks in the ultraviolet at a 128 nm, shown in comparison to Xenon and Kypton in Figure [183]. The light yield collected by the optical detector depends on the argon purity, the electric field, the dE/dx and particle type, averaging at the tens of thousands of photons per MeV. The de-excitation of Rydberg dimers in the argon is responsible for the scintillation light. Rydberg dimers exist in two states: singlets and a triplets. The time constant for the singlet radiative decay is 6 ns, resulting in a prompt component for the scintillation light. The decay of the triplet is

delayed by intersystem crossing, producing a slow component with a time constant of $\sim$ 1500 ns. "Self-trapped exciton luminescence" and "recombination luminescence" are the two processes responsible for the creation of the Rydberg dimers. In the first process, a charged particle excites an argon atom which becomes self-trapped in the surrounding bulk of argon, forming a dimer; the dimer is in the singlet state 65% of the times and in the triplet state 35% of the times. In case of recombination luminescence, the charged particle transfers enough energy to ionize the argon. The argon ion forms a charged argon dimer state, which quickly recombines with the thermalized free electron cloud. Excimer states are produced in the recombination, roughly half in the singlet and half in the triplet state. The light yield dependency on the electric field, on the dE/dx and particle type derives from the role of free charge in the recombination luminescence process. The spacial separation between the argon ions and the free electron cloud depends on the electric field. On one hand, a strong electric field diminishes the recombination probability, leading to a smaller light yield; on the other, it increases the free charge drifting towards the anode plane. Hence, the amount of measurable charge and light anti-correlates as a function of the electric field. Ionizing particles in the argon modify the local density of both free electrons and ions depending on their dE/dx. Since the recombination rate is proportional to the square of the local ionization density, highly ionizing particles boost recombination and the subsequent light yield compared to MIPs. The possibility to leverage this dependency for pulseshape-based particle identification has been shown in [186], [187].

Effects Modifying the Light Yield

The production mechanism through emission from bound excimer states implies that argon is transparent to its own scintillation light. In fact, the photons emitted from these metastable states are not energetic enough to re-excite the argon bulk, greatly suppressing absorption mechanisms. In a LArTPC however, several processes mod-

ify the light yield in between the location where light is produced and the optical detector. In a hypothetical pure tank of argon, Rayleigh scattering would be the most important processes modifying the light yield. Rayleigh scattering changes the path of light propagation in argon, prolonging the time between light production and detection. The scattering length has been measured to be 66 cm [191] , shorter than the theoretical prediction of $\sim$ 90 cm [190]; this value is short enough to be relevant for the current size of LArTPCs detectors. In fact, Rayleigh scattering worsen the resolution on t_0, the start time for charge drifting, and alters the light directionality, complicating the matching between light and charge coming from the same object in case of multiple charged particles in the detector.

Traces of impurities in argon such as oxygen, water and nitrogen also affect the light yield, mainly via absorption and quenching mechanisms. Absorption occurs as the interaction of a 128 nm photon directly with the impurity dissolved in the liquid argon. Differently, quenching occurs as the interaction of an argon excimer and an impurity, where the excimer transfers its excitation to the impurity and dissociates non-radiatively. Given this mechanism, it is evident how quenching is both a function of the impurity concentrations and the excimer lifetime. Since the triplet states live much longer than the singlet states, quenching occurs mainly on triplet states, affecting primarily the slow component of the light, reducing the scintillation yield and a shortening of the scintillation time constants.

The stringent constraints for the electron life time limit the presence of oxygen and water to such a low level that both absorption and quenching on these impurity is not expected to be significant [210]. Contrarily, the nitrogen level is not bound by the electron life time constraints – nitrogen being an inert gas, expensive to filter. Thus, nitrogen is often present at the level provided by the vendor. The effects of nitrogen on argon scintillation light have been studied in the WArP R&D program and at several test stands. The quenching process induced by nitrogen in liquid Ar has

been measured to be proportional to the nitrogen concentration, with a rate constant of ~ 0.11 μs^{-1} ppm^{-1}; appreciable decreasing in lifetime and relative amplitude of the slow component have been shown for contamination as high as a few ppm of nitrogen [2]. For a nitrogen concentration of 2 parts per million, typical of the current generation of LArTPC, the attenuation length due to nitrogen has been measured to be $\sim$30 meters [46].

Wavelength Shifting of LAr Scintillation Light

Liquid argon scintillation light is invisible for most optical detectors deployed in LArTPC, such as cryogenic PMTs and SiPMs, since a wavelength of 128 nm is generally too short to be absorbed from most in glasses, polymers and semiconductor materials. Research on prototype SiPMs absorbing directly VUV light and their deployment in noble gasses experiment is ongoing but not mature [65]. Thus, experiments need to shift the wavelength of scintillation light to be able to detect it. Albeit deployed in different ways, neutrinos and dark matter experiments commonly use 1,1,4,4-tetraphenyl-butadiene (TPB) to shift the scintillation light. TPB, whose chemical structure is shown in figure , absorbs the vacuum ultraviolet (VUV) light and emits in the visible at $\sim$ 425 nm [231], with a ratio of visible photon emitted per VUV photon absorbed of $\sim$1.2:1 [36].

Neutrino experiments typically coat their optical detector system evaporating a layer of TPB either directly on the PMTs glass surface or on acrylic plates mounted in front of the PMTs cite microboone; this technique allows the fast detection light coming directly from the neutrino interaction. Dark matter experiments typically evaporate TPB on reflective foils mounted on the inside walls of the sensitive volume and detect the light after it has been reflected; this technique leads to a higher and more uniform light yield, though scattering effects for both the visible and VUV light augment the propagation time and hinder directionality informationsome DM

detector . In order to take advantage of both these techniques, hybrid systems with PMT coating and foils are being considered for the next generation of large neutrino detectors cite SBND?.

0.1.5   Signal Processing and Event Reconstruction

In this section we illustrate the processing and reconstruction chain of the TPC signals, from the pulses on the sense wire to the construction of three dimensional objects with associated calorimetry.

Deconvolution. Induction and collection planes have different field responses, given the different nature of the signals on these planes: the wires on the induction planes see inductive signal of the drifting charge, while the wires on the collection planes see the current derived from the charge entering the conductor. Thus, signals on the induction plane are bi-polar pulse and signal on the collection plane are unipolar pulses, see Figure ADD PULSES FIGURE. The first step in signal processing is deconvolution, that is a series of off-line algorithms geared towards undoing the detector effects. The result of the deconvolution step is the production of a comparable set waveforms on all planes presenting unipolar, approximately gaussian-like pulses. Signal from all planes are treated on equal footage beyond this point. Some LArTPC apply noise filtering in the frequency domain just after the deconvolution to clean up wire cross talk. Since signals from the LArIAT TPC are extremely clean, noise filtering is not necessary.

Hit Reconstruction. The second stage of the signal processing is the reconstruction of hits, indicating an energy deposition in the detector. A peak finder scans the deconvolved TPC waveforms for each wire on the whole readout time looking for spikes above the waveform's baseline. It then fits these peaks with gaussian shapes

and stores the fit parameters such as the quality of the fit, the peak time, height and area under the gaussian fit. The information resulting fron this process a single spike form a single reconstructed "hit". The next steps in the event reconstruction chain will then decide if rejecting hits with poor fits. It is important to notice how the height and width of the hit depend on the topology of the event: for example, a particle running parallel to the wire planes will leave a series of sharp hits on many consecutive wires, while a particle traveling towards the planes will leave a long, wide hit on very few wires. The height of the hits and their integral is proportional to the charge collected on the wire, so it depends on the particle type.

The event reconstruction chain uses collection of hits to form more complex objects associated with the particles in the detector. The development of different approaches to accomplish this task is an extremely hot topic in LArTPC event reconstruction which spans from more traditional approaches such as line-clustering [?] argoneut paper to the use of machine learning tools [?] KAZU'S paper. Generally speaking, the scope of hit clustering and event reconstruction to provide shower-like or track like-objects with an associated energy reconstruction. This is because different particles have different topology in the detector – electrons and photon create electromagnetic showers, resulting in shower-like topologies, while muons and hadrons leave track-like signals. For the scope of these thesis, we will describe only LArIAT's approach to track reconstruction even if we recognize the breath of LArTPC event reconstruction is much wider. We are interested in the reconstruction of pions and kaons in the active volume, whose topology is track-like.

Track Reconstruction The track reconstruction used in this analysis is performed by the Pandora reconstruction package [55]. Pandora utilizes reconstruction algorithms that are tuned separately to identify tracks likely to be cosmic rays, and those likely to be from neutrino interactions. Both processes begin similarly. First, hits are grouped into 2D clusters on each plane with preference given to preserving the

purity of the cluster with respect to its parent particle rather than the completeness In other words, it?s preferable to miss some of the true initial particle that deposited the energy and to produce an object with only one true parent particle, rather than to produce a mostly complete, reconstructed object that combines multiple parent particle into one cluster. From here, the 3 planes are scanned for 3 consistent, highly linear clusters (one cluster per plane) that overlap in the shared time coordinate. Matching of these clusters proceeds as follows: for every pair of 2 clusters in 2 planes that overlap in time, a predictive position for the points of the 3rd cluster in the 3rd plane is calculated. The results of all these calculations are then compared to the 3rd candidate cluster and a ? 2 value is calculated to reflect the quality of the fit. From here, neutrino-specific algorithms utilize a number of direction and proximity metrics to assess the likelihood that each reconstructed track originated from a neutrino interaction. There tracks are then assigned a cosmic tag if they are exiting and entering the detector. They are also cosmic tagged if they are not in coincidence with a beam flash. The remaining tracks without a cosmic tag are neutrino interaction track candidates One obstacle track reconstruction faces are regions of the anode plane where wires are not functioning properly. These regions are called ?dead wires? and are shown in

0.2 The Intensity Frontier Program

0.2.1 SBN: Neutrino Interaction and Detection

0.2.2 DUNE: Rare Decay Searches

DUNE will achieve a wide non-accelerator physics program. The key elements for a rare decay experiment are: massive active volume, long exposure, high identification efficiency and low background. Figure 1 shows the current best experimental limits

on nucleon decay lifetime over branching ratio (dots). Historically, the dominant technology used in these searches has been water Cherenkov detectors: all the best experimental limits on every decay mode are indeed set by Super-Kamiokande [?, ?]. It is particularly important to notice that the kaon energy for the proton decay mode $p \to K^+ \bar{\nu}$ is under Cherenkov threshold. Super-Kamiokande set the limit on the lifetime for the $p \to K^+ \bar{\nu}$ mode by relying exclusively on photons from nuclear de-excitation. For this reason, an attractive alternative approach to identifying nucleon decay is the use of a Liquid Argon Time Projection Chamber (LArTPC).

LArTPCs can complement nucleon decay searches in modes where water Cherenkov detectors are less sensitive, especially $p \to K^+ \bar{\nu}$. According to [?], DUNE will have an active volume large enough, have sufficient shielding from the surface, and will run for lengths of time sufficient to compete with Hyper-K, opening up the opportunity for the discovery of nucleon decay.
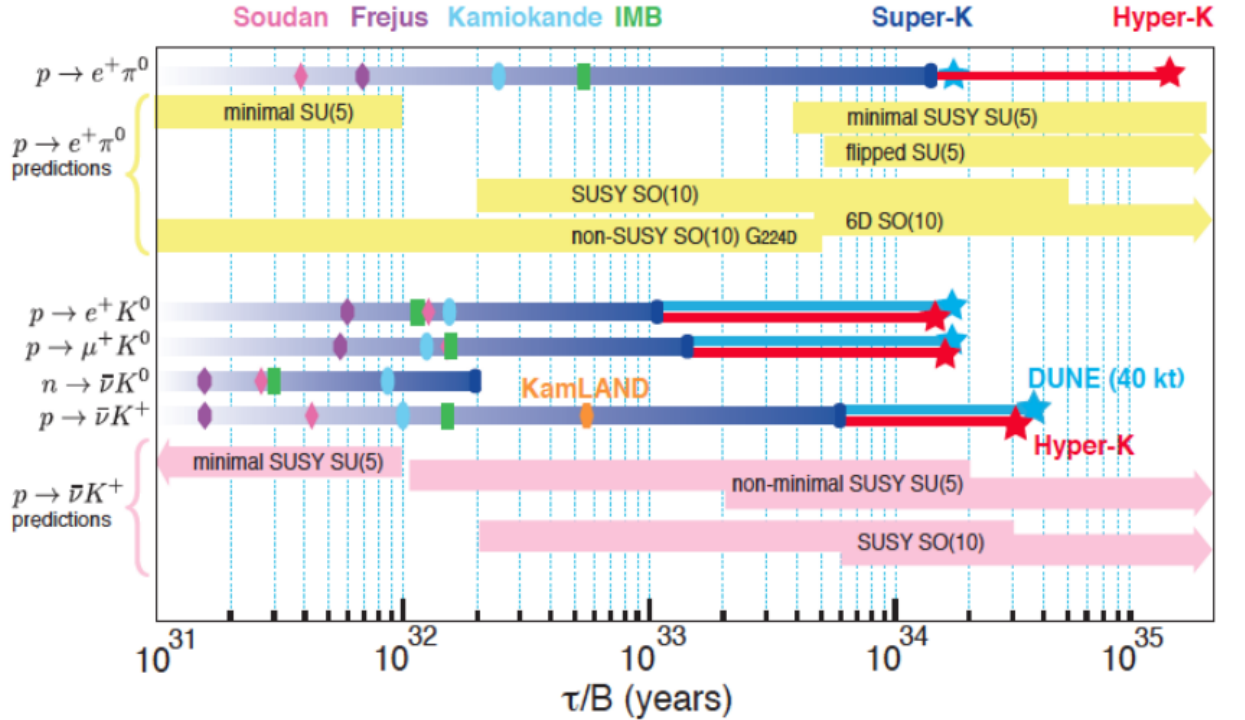

Figure 1: Proton decay lifetime limits from passed and future experiments.
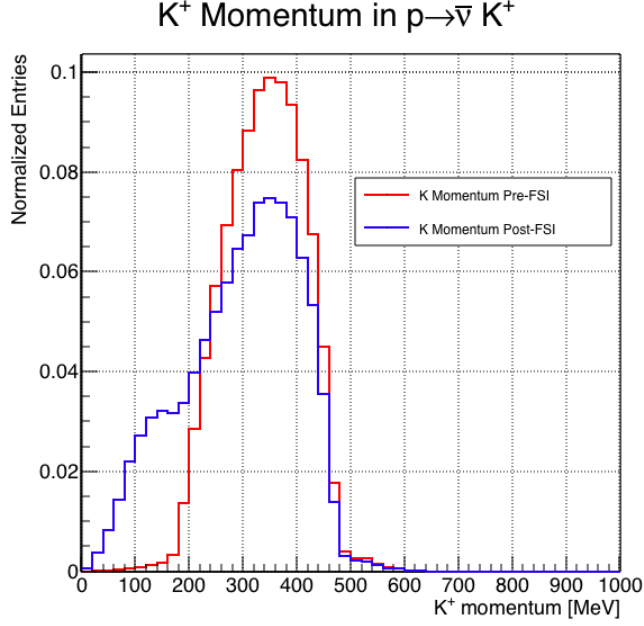
Figure 2: Momentum of the kaon outgoing a proton decay event as simulated by the Genie 2.8.10 event generator in argon. The red line represent the kaon momentum distribution before undergoing the simulated final state interaction inside the argon nucleus, while the blue line represents the momentum distribution after FSI.

0.2.3   Enabling the next generation of discoveries: LArIAT

LArIAT, a small Liquid Argon Time Projection Chamber (LArTPC) in a test beam, is designed to perform an extensive physics campaign centered on charged particle cross section measurements while characterizing the detector performance for future LArTPCs. LArTPC represents one of the most advanced experimental technologies for physics at the Intensity Frontier due to its full 3D-imaging, excellent particle identification and precise calorimetric energy reconstruction. This complex technology however needs a thorough calibration and dedicated measurements of some key quantities to achieve the precision required for the next generation of discoveries at the Intensity Frontier which LArIAT can provide.

The LArIAT LArTPC is deployed in a dedicated calibration test beamline at Fermilab. We use the LArIAT beamline to characterize the charge particles before they enter the TPC: the particle type and initial momentum is known from beamline in-

formation. The precise calorimetric energy reconstruction of the LArTPC technology enables the measurement of the total differential cross section for tagged hadrons. The Pion-Nucleus and Kaon-Nucleus total hadronic interaction cross section have never been measured before in argon and they are a fundamental step to shed light on light meson interaction in nuclei. Additionally, these measures provides a key input to neutrino physics and proton decay studies in future LArTPC experiments like SBN and DUNE. add paragraph on all wonderful things lariat can do... some event displays would be nice!

ADD genie proton decay kaon distribution and lariat beamline overlaied The signature of a proton decay event in the "LAr golden mode" is the presence of a single kaon of about 400 MeV in the detector.

Bibliography

[1] Precision electroweak measurements on the z resonance. *Physics Reports*, 427(5):257 – 454, 2006.

[2] R Acciarri, M Antonello, B Baibussinov, M Baldo-Ceolin, P Benetti, F Calaprice, E Calligarich, M Cambiaghi, N Canci, F Carbonara, F Cavanna, S Centro, A G Cocco, F Di Pompeo, G Fiorillo, C Galbiati, V Gallo, L Grandi, G Meng, I Modena, C Montanari, O Palamara, L Pandola, G B Piano Mortari, F Pietropaolo, G L Raselli, M Roncadelli, M Rossella, C Rubbia, E Segreto, A M Szelc, S Ventura, and C Vignoli. Effects of nitrogen contamination in liquid argon. *Journal of Instrumentation*, 5(06):P06003, 2010.

[3] R. Acciarri et al. Demonstration and Comparison of Operation of Photomultiplier Tubes at Liquid Argon Temperature. *JINST*, 7:P01016, 2012.

[4] A. Aguilar-Arevalo et al. Evidence for neutrino oscillations from the observation of anti-neutrino(electron) appearance in a anti-neutrino(muon) beam. *Phys. Rev.*, D64:112007, 2001.

[5] A. A. Aguilar-Arevalo et al. Improved Search for $\bar{\nu}_\mu \to \bar{\nu}_e$ Oscillations in the MiniBooNE Experiment. *Phys. Rev. Lett.*, 110:161801, 2013.

[6] C. Anderson et al. The ArgoNeuT Detector in the NuMI Low-Energy beam line at Fermilab. *JINST*, 7:P10019, 2012.

[7] C. Andreopoulos et al. The GENIE Neutrino Monte Carlo Generator. *Nucl. Instrum. Meth.*, A614:87–104, 2010.

[8] D. Ashery, I. Navon, G. Azuelos, H. K. Walter, H. J. Pfeiffer, and F. W. Schlepütz. True absorption and scattering of pions on nuclei. *Phys. Rev. C*, 23:2173–2185, May 1981.

[9] C. Athanassopoulos et al. Evidence for nu(mu) → nu(e) neutrino oscillations from LSND. *Phys. Rev. Lett.*, 81:1774–1777, 1998.

[10] Borut Bajc, Junji Hisano, Takumi Kuwahara, and Yuji Omura. Threshold corrections to dimension-six proton decay operators in non-minimal {SUSY} su(5) {GUTs}. *Nuclear Physics B*, 910:1 – 22, 2016.

[11] BASF Corp. 100 Park Avenue, Florham Park, NJ 07932 USA.

[12] A. Bodek and J. L. Ritchie. Further studies of fermi-motion effects in lepton scattering from nuclear targets. *Phys. Rev. D*, 24:1400–1402, Sep 1981.

[13] D. V. Bugg, R. S. Gilmore, K. M. Knight, D. C. Salter, G. H. Stafford, E. J. N. Wilson, J. D. Davies, J. D. Dowell, P. M. Hattersley, R. J. Homer, A. W. O'dell, A. A. Carter, R. J. Tapper, and K. F. Riley. Kaon-nucleon total cross sections from 0.6 to 2.65 gev/ *c. Phys. Rev.*, 168:1466–1475, Apr 1968.

[14] A. S. Carroll, I. H. Chiang, C. B. Dover, T. F. Kycia, K. K. Li, P. O. Mazur, D. N. Michael, P. M. Mockett, D. C. Rahm, and R. Rubinstein. Pion-nucleus total cross sections in the (3,3) resonance region. *Phys. Rev. C*, 14:635–638, Aug 1976.

[15] D. Casper. The nuance neutrino physics simulation, and the future. *Nuclear Physics B - Proceedings Supplements*, 112(1-3):161–170, nov 2002.

[16] A. Cervera, A. Donini, M.B. Gavela, J.J. Gomez Cádenas, P. Hernández, O. Mena, and S. Rigolin. Golden measurements at a neutrino factory. *Nuclear Physics B*, 579(1-2):17–55, jul 2000.

[17] ATLAS Collaboration. Observation of a new particle in the search for the standard model higgs boson with the ATLAS detector at the LHC. *Physics Letters B*, 716(1):1–29, sep 2012.

[18] CMS Collaboration. Observation of a new boson at a mass of 125 gev with the cms experiment at the lhc. *Physics Letters B*, 716(1):30 – 61, 2012.

[19] Savas Dimopoulos, Stuart Raby, and Frank Wilczek. Proton Decay in Supersymmetric Models. *Phys. Lett.*, B112:133, 1982.

[20] D. Drakoulakos et al. Proposal to perform a high-statistics neutrino scattering experiment using a fine-grained detector in the NuMI beam. 2004.

[21] A Ereditato, C C Hsu, S Janos, I Kreslo, M Messina, C Rudolf von Rohr, B Rossi, T Strauss, M S Weber, and M Zeller. Design and operation of argontube: a 5 m long drift liquid argon tpc. *Journal of Instrumentation*, 8(07):P07002, 2013.

[22] Torleif Ericson and Wolfram Weise. *Pions and Nuclei (The International Series of Monographs on Physics)*. Oxford University Press, 1988.

[23] A.A. Aguilar-Arevalo et al. The miniboone detector. *Nuclear Instruments and Methods in Physics Research Section A: Accelerators, Spectrometers, Detectors and Associated Equipment*, 599(1):28 – 46, 2009.

[24] Antonio Bueno et al. Nucleon decay searches with large liquid argon TPC detectors at shallow depths: atmospheric neutrinos and cosmogenic backgrounds. *Journal of High Energy Physics*, 2007(04):041–041, apr 2007.

[25] A.S. Clough et al. Pion-nucleus total cross sections from 88 to 860 MeV. *Nuclear Physics B*, 76(1):15–28, jul 1974.

[26] B.W. Allardyce et al. Pion reaction cross sections and nuclear sizes. *Nuclear Physics A*, 209(1):1 – 51, 1973.

[27] C Athanassopoulos et al. The liquid scintillator neutrino detector and LAMPF neutrino source. *Nuclear Instruments and Methods in Physics Research Section A: Accelerators, Spectrometers, Detectors and Associated Equipment*, 388(1-2):149–172, mar 1997.

[28] F. Binon et al. Scattering of negative pions on carbon. *Nuclear Physics B*, 17(1):168 – 188, 1970.

[29] L. Aliaga et al. Minerva neutrino detector response measured with test beam data. *Nuclear Instruments and Methods in Physics Research Section A: Accelerators, Spectrometers, Detectors and Associated Equipment*, 789:28 – 42, 2015.

[30] M Adamowski et al. The liquid argon purity demonstrator. *Journal of Instrumentation*, 9(07):P07005, 2014.

[31] P. Vilain et al. Coherent single charged pion production by neutrinos. *Physics Letters B*, 313(1-2):267–275, aug 1993.

[32] H Fenker. Standard beam pwc for fermilab. Technical report, Fermi National Accelerator Lab., Batavia, IL (USA), 1983.

[33] H Fesbach. Theoretical nuclear physics: Nuclear reactions. 1992.

[34] J. A. Formaggio and G. P. Zeller. From ev to eev: Neutrino cross sections across energy scales. *Rev. Mod. Phys.*, 84:1307–1341, Sep 2012.

[35] E. Friedman et al. K+ nucleus reaction and total cross-sections: New analysis of transmission experiments. *Phys. Rev.*, C55:1304–1311, 1997.

[36] V.M. Gehman, S.R. Seibert, K. Rielage, A. Hime, Y. Sun, D.-M. Mei, J. Maassen, and D. Moore. Fluorescence efficiency and visible re-emission spectrum of tetraphenyl butadiene films at extreme ultraviolet wavelengths. *Nuclear Instruments and Methods in Physics Research Section A: Accelerators, Spectrometers, Detectors and Associated Equipment*, 654(1):116 – 121, 2011.

[37] Howard Georgi and S. L. Glashow. Unity of all elementary-particle forces. *Phys. Rev. Lett.*, 32:438–441, Feb 1974.

[38] D.Y. Wong (editor) G.L. Shaw (Editor). *Pion-nucleon Scattering*. John Wiley & Sons Inc, 1969.

[39] Glassman High Voltage, Inc., Precision Regulated High Voltage DC Power Supply.

[40] D S Gorbunov. Sterile neutrinos and their role in particle physics and cosmology. *Physics-Uspekhi*, 57(5):503, 2014.

[41] S. Hansen, D. Jensen, G. Savage, E. Skup, and A. Soha. Fermilab test beam multi-wire proportional chamber tracking system upgrade. June 2014. International Conference on Technology and Instrumentation in Particle Physics (TIPP 2014).

[42] Peter W. Higgs. Broken symmetries and the masses of gauge bosons. *Physical Review Letters*, 13(16):508–509, oct 1964.

[43] P.W. Higgs. Broken symmetries, massless particles and gauge fields. *Physics Letters*, 12(2):132–133, sep 1964.

[44] H J Hilke. Time projection chambers. *Reports on Progress in Physics*, 73(11):116201, 2010.

[45] C. Jarlskog. A basis independent formulation of the connection between quark mass matrices, CP violation and experiment. *Zeitschrift für Physik C Particles and Fields*, 29(3):491–497, sep 1985.

[46] B J P Jones, C S Chiu, J M Conrad, C M Ignarra, T Katori, and M Toups. A measurement of the absorption of liquid argon scintillation light by dissolved nitrogen at the part-per-million level. *Journal of Instrumentation*, 8(07):P07011, 2013.

[47] Cezary Juszczak, Jarosław A. Nowak, and Jan T. Sobczyk. Simulations from a new neutrino event generator. *Nuclear Physics B - Proceedings Supplements*, 159:211–216, sep 2006.

[48] D. I. Kazakov. Beyond the standard model: In search of supersymmetry. In *2000 European School of high-energy physics, Caramulo, Portugal, 20 Aug-2 Sep 2000: Proceedings*, pages 125–199, 2000.

[49] Dae-Gyu Lee, R. N. Mohapatra, M. K. Parida, and Merostar Rani. Predictions for the proton lifetime in minimal nonsupersymmetric so(10) models: An update. *Phys. Rev. D*, 51:229–235, Jan 1995.

[50] Ettore Majorana. Teoria simmetrica dell'elettrone e del positrone. *Il Nuovo Cimento*, 14(4):171–184, apr 1937.

[51] FM Newcomer, S Tedja, R Van Berg, J Van der Spiegel, and HH Williams. A fast, low power, amplifier-shaper-discriminator for high rate straw tracking systems. *IEEE Transactions on Nuclear Science*, 40(4):630–636, 1993.

[52] Emmy Noether. Invariant variation problems. *Transport Theory and Statistical Physics*, 1(3):186–207, jan 1971.

[53] S. Pascoli, S.T. Petcov, and A. Riotto. Leptogenesis and low energy cp-violation in neutrino physics. *Nuclear Physics B*, 774(1):1 – 52, 2007.

[54] C. Patrignani et al. Review of Particle Physics. *Chin. Phys.*, C40(10):100001, 2016.

[55] B. Pontecorvo. Neutrino Experiments and the Problem of Conservation of Leptonic Charge. *Sov. Phys. JETP*, 26:984–988, 1968. [Zh. Eksp. Teor. Fiz.53,1717(1967)].

[56] Steve Ritz et al. Building for Discovery: Strategic Plan for U.S. Particle Physics in the Global Context. 2014.

[57] L.M. Saunders. Electromagnetic production of pions from nuclei. *Nucl. Phys., B7: 293-310(1968).*

[58] Sigma-Aldrich, P.O. Box 14508, St. Louis, MO 63178 USA.

[59] D.R.O. Morrison N. Rivoire V. Flaminio, W.G. Moorhead. Compilation of Cross Sections I: π^+ and π^- Induced Reactions. *CERN-HERA*, pages 83–01, 1983.

[60] D.R.O. Morrison N. Rivoire V. Flaminio, W.G. Moorhead. Compilation of Cross Sections II: K^+ and K^- Induced Reactions. *CERN-HERA*, pages 83–02, 1983.

[61] Hermann Weyl. Gravitation and the electron. *Proceedings of the National Academy of Sciences of the United States of America*, 15(4):323–334, 1929.

[62] Colin et al Wilkin. A comparison of pi+ and pi- total cross-sections of light nuclei near the 3-3 resonance. *Nucl. Phys.*, B62:61–85, 1973.

[63] D. H. Wright and M. H. Kelsey. The Geant4 Bertini Cascade. *Nucl. Instrum. Meth.*, A804:175–188, 2015.

[64] C. S. Wu, E. Ambler, R. W. Hayward, D. D. Hoppes, and R. P. Hudson. Experimental test of parity conservation in beta decay. *Phys. Rev.*, 105:1413–1415, Feb 1957.

[65] N Yahlali, L M P Fernandes, K Gonzlez, A N C Garcia, and A Soriano. Imaging with sipms in noble-gas detectors. *Journal of Instrumentation*, 8(01):C01003, 2013.

[66] T. Yanagida. Horizontal symmetry and masses of neutrinos. *Progress of Theoretical Physics*, 64(3):1103–1105, sep 1980.